Rare earth oxides in zirconium dioxide: How to turn a wide band gap metal oxide into a visible light active photocatalyst

Rare Earth Oxides in Zirconium Dioxide: How to Turn a Wide Band Gap Metal Oxide into a Visible Light Active Photocatalyst

Chiara Gionco[a], Maria C. Paganini[a], Elio Giamello[a,*], Olga Sacco[b], Vincenzo Vaiano[b], Diana Sannino[b]

[a] *Department of Chemistry, University of Torino,Via Giuria 7, 10125, Torino, Italy*

[b] *Department of Industrial Engineering, University of Salerno, Via Giovanni Paolo II 132, 84084 Fisciano (SA), Italy*

Article history:

Received 26 May 20xx

Revised 9 June 20xx

Accepted 29 June 20xx

Available online

Abstract

In the present study, we investigated the effect of cerium and erbium doping in zirconium dioxide matrix. We synthesized doped samples using hydrothermal process. The amount of dopant used was 0.5, 1 and 5% molar (rare earth oxide over zirconium dioxide). The samples have been studied via X Ray Diffraction measurements for the structural characterization. UV visible diffuse reflectance was used for the optical analysis, Branauer-Emmett-Teller (BET) model for the measurement of the surface area. Finally the samples have been analysed via electron paramagnetic resonance (EPR) for the electronic characterization. Then we tested the new synthetized materials to determine their photocatalytic activity in the reaction of degradation of methylene blue performed under irradiation by diodes (LEDs) emitting exclusively visible light.

Key words: 3rd generation photocatalysts, Zirconium dioxide, rare earth ions, dyes mineralization.

*** Corresponding author.** Tel: +390116707574; Fax: +396707578; E-mail: elio.giamello@unito.it

This work was supported by the CARIPLO Foundation with the Advanced Materials Grant 2013 "Development of second generation photocatalysts for energy and environment" and by the Local Funding of the University of Torino call_2014_L2_126.

1. Introduction

After the experiment of light induced water splitting by Honda and Fujishima in 1972, the concept of photocatalysis became familiar to the scientific community. Since then, the main routes of the experimental research in this field were essentially two. The first route seeks the advent of a new energetic system aiming to achieve an efficient photochemical production of hydrogen from water and the photoreduction of CO_2 (artificial photosynthesis). The second one concerns environmental chemistry as it deals with the remediation of pollutants in waters and in the atmosphere. In this second case, the oxidative capability of the photocatalyst is critical. For this reason titanium dioxide (which shows an optimal flat band potential for oxidation) has been the dominant photochemical system in this kind of environmental applications for many years. A further application of increasing importance concerns the role of titanium dioxide and other photocatalysts in determining alternative routes to traditional synthetic processes of organic chemistry both at laboratory and industrial level [1]. All the mentioned applications, however, employ UV light for irradiation [2, 3]. The UV frequencies are in fact necessary to create the electron-hole photoinduced separation (excitation from valence band to conduction band, separated by about 3.2 eV) which is the starting act of the whole reactivity. However, after years of successful applications of TiO_2 photocatalysis for pollutants removal, the need of UV light to perform photocatalytic reactions started to be seen as a limit of this process. Also in view of the construction of larger scale photocatalytic plants the use of sunlight (quite poor in the UV component and rich in both visible and NIR light) started to become an unavoidable necessity.

Applications of visible light in photocatalytic reactions face an apparently irreconcilable contradiction. Using heterogeneous photocatalyst with lower band gap value, in fact, allows, on the one hand, the charge separation with lower energy photons (visible) but implies, on the other hand, to have less effective flat band potentials for Valence Band (VB) and Conduction Band (CB) therefore limiting (or even canceling) the photocatalytic activity.

To overcome this clear contradiction new generations of photocatalyst have been prepared and tested since the beginning of this century. The second generation of photocatalyst was essentially based on titanium dioxide modified with various dopants. [4, 5].The most important member of this family, at least for historical reasons, is nitrogen doped TiO_2, proposed by Ashai in 2001 [6] and whose (moderate) effects under visible light have been rationalized later basing on the electronic structure of the system

The third generation of photocatalysts tries to go beyond titanium dioxide and was initially a prediction proposed by N. Serpone and A. Emeline. This was based on the idea of a wide band gap semiconductor (hence with excellent flat band potentials) containing extra electronic levels at intermediate energy in the band gap [7, 8] capable of allowing the transition of electrons from the VB to the CB with a double excitation. An example of such a behavior has been recently proposed by some of us reporting the properties of cerium doped zirconium dioxide. ZrO_2 has a band gap energy wider than that of TiO_2 (about 5 eV [9]) and better flat band potentials (in particular the reduction potential of the CB, see Scheme 1) than titania. Despite the band gap value, corresponding to high energy UV photons, we have shown in the case of Ce-doped ZrO_2, that visible light is capable to promote electrons in the CB creating holes in the valence band. This effect, that was monitored via Electron Paramagnetic Resonance spectroscopy following the fate of the photoexcited charge carriers, is certainly not huge in quantitative terms but remains conceptually significant in terms of proof of concepts [10]. Responsible of these properties, as also shown by theoretical modelling, are the Ce^{4+} 4f empty levels that allow the described electron excitation. The sol-gel method adopted for the synthesis favors the intimate mixture of the components and the formation of isolated cerium centers in the lattice. Though uncommon, the presence of rare earth ions in photocatalytic systems is not totally new. In recent years, for instance, A. Zaleska and coworkers have reported the photocatalytic properties of titanium dioxide doped with various rare earth ions [11].

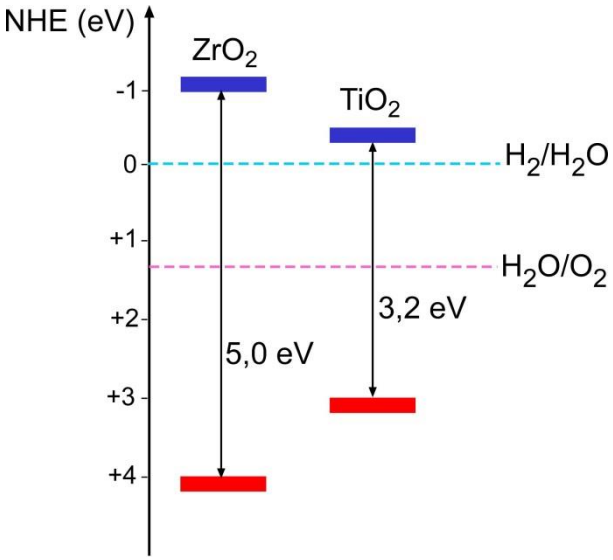

Scheme 1: Flat band potentials of ZrO_2 [9] and TiO_2 [12]

With the present work, we intended to test the real photocatalytic properties of this novel family of

materials investigating two families of zirconium dioxide doped with Cerium and Erbium ions, respectively, at various quantitative levels. The two rare earth elements were selected in order to test ions rich od 4f electrons (Er^{3+}) or with 4f levels completely empty (Ce^{4+}). In the first part of the paper, a basic characterization of the structural, optical and photochemical properties of the prepared materials is reported. The second part is devoted to the investigation of their photocatalytic activity in the reaction of degradation of methylene blue performed under irradiation by diodes (LEDs) emitting exclusively visible light. This was done in order to verify the potentiality of the novel systems in photocatalytic reactions under low energy photons (i.e. in the absence of UV components) that is essential for future applications under true solar light.

2. Experimental

2.1. Synthesis of catalysts

In this work samples of zirconium dioxide doped with rare earth (RE, RE=Ce, Er) ions were prepared. All reactants employed were purchased from Aldrich and were used without any further purification treatment.

The samples were prepared via a hydrothermal process starting from a 1.0 *M* aqueous solution containing the stoichiometric ratio of $ZrOCl_2 \cdot 8H_2O$ and $Ce(SO_4)_2$ or $Er(NO_3)_3 \cdot 5H_2O$. The *pH* was then adjusted to 11 using a 4.0 *M* NaOH aqueous solution, inducing the formation of a gel. The gel was then transferred into a 125 ml Teflon-lined stainless steel autoclave, 70% filled, which was heated in oven at 448 K overnight. The precipitates were then centrifuged and washed several times, then dried at 333 K. For comparison pure ZrO_2 was prepared with the same procedure.

For each dopant (CeO_2 or Er_2O_3), samples of different concentration, namely 0.5%, 1% and 5% molar, were prepared. Samples will be labeled as Z for bare zirconia, CZ05 and EZ05 for zirconia doped with 0.5% of cerium and erbium respectively, CZ1 and EZ1 for zirconia doped with 1% of cerium and erbium respectively, and finally CZ5 and EZ5 for zirconia doped with 5% of cerium and erbium respectively.

2.2. Characterization of catalyst

X-Ray Diffraction (XRD) patterns were recorded with a PANalytical PW3040/60 X'Pert PRO MPD

using a copper Kα radiation source (0.15418 nm) and a Bragg Brentano geometry. X'Pert High-Score software was used for data handling.

Diffuse Reflectance Spectroscopy (DRS) data were recorded using a Varian Cary 5000 spectrometer, coupled with an integration sphere for diffuse reflectance studies, using a Carywin-UV/scan software. A sample of PTFE with 100% reflectance was used as reference.

Electron Paramagnetic Resonance (EPR) spectra were recorded at room temperature and at liquid nitrogen temperature (77 K). They were run on a X-band CW-EPR Bruker EMX spectrometer equipped with a cylindrical cavity operating at 100 kHz field modulation. The effect of light on EPR spectra was investigated using a 1600 W Xenon lamp (Oriel Instruments) equipped with a IR water filter. To simulate the solar spectrum a 400 nm cut-off filter has been used for selected experiments.

Surface area measurements were carried out on a Micromeritics ASAP 2020 using the Branauer-Emmett-Teller (BET) model on the N_2 adsorption measurement and 9 p/p^0 points. Prior to the adsorption run, all the samples were outgassed at 573 K for 3 h.

Photocatalytic experiments were carried out with a pyrex tubular photoreactor (Internal diameter = 2.5 cm) equipped with an air distributor device (Q_{air} = 150 mL/min (STP)), a magnetic stirrer to maintain the photocatalyst suspended in the aqueous solution and a temperature controller [13]. The photoreactor was irradiated by a strip composed of 30 white light LEDs (nominal power: 6 W) with wavelength emission in the range 400–800 nm (with a maximum centered at about 475 nm) [14, 15].

The LEDs strip was positioned around the reactor to assure uniform illumination of the reaction volume.

In a typical photocatalytic test, 3 g/L of photocatalyst was suspended in 100 mL solution. The system was kept in dark condition for 3 h to reach methylene blue (MB) adsorption equilibrium on the catalyst surface, and then the photocatalytic reaction was initiated by the LEDs lighting. Liquid samples were taken at regular time intervals during the test and centrifuged for 20 minutes at 4000 rpm for removing the photocatalyst particles. The centrifuged samples were analyzed to determine the change of MB concentration, measured with a Perkin Elmer UV-Vis spectrophotometer at λ = 663 nm. The initial concentration of MB in the photocatalytic tests was equal to 7 mg/L. The total organic carbon (TOC) of the aqueous samples was measured by the high temperature combustion method [16] on a catalyst (Pt/Al_2O_3) in a tubular flow microreactor operated at 953 K, with a stream of hydrocarbon free air to

oxidize the organic carbon. Laboratory apparatus consisted of mass flow controllers (Brooks) operating on each gas; an injection system; a NDIR continuous analyser (Hartmann & Braun Uras 10E) for measurements of CO and CO_2 concentrations at the combustion reactor outlet and a paramagnetic analyser (Hartmann & Braun Magnos 6G) for continuous monitoring of O_2.

3. Results and discussion

Figure 1 shows the XRD patterns obtained for the pure zirconia sample, the Ce doped (Fig. 1a) and Er doped (Fig. 1b) ZrO_2 samples.

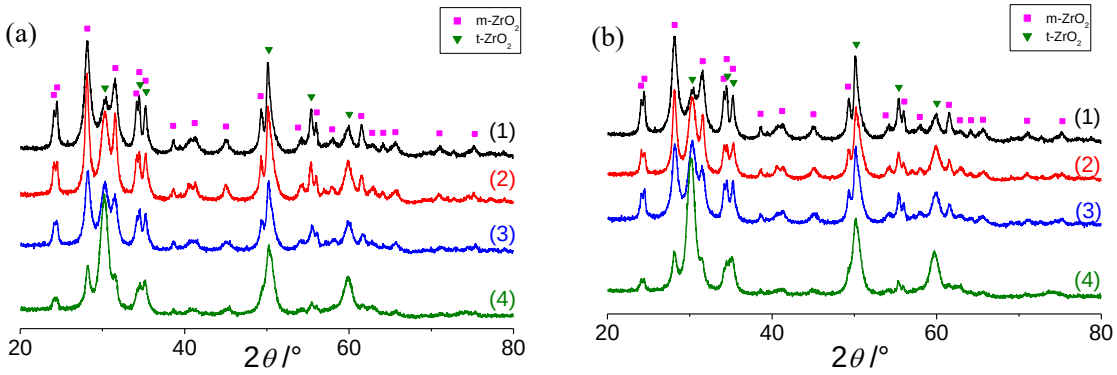

Figure 1. XRD patterns of 1) pure ZrO_2 (black) and RE-doped ZrO_2 (panel a: RE=Ce, panel b: RE=Er) with increasing concentration of RE dopant: 2) 0.5 mol% (red), 3) 1 mol% (blue), 4) 5 mol% (green).

The pure ZrO_2 sample is crystalline, and presents two zirconia polymorphs: the tetragonal and the monoclinic phase. Increasing the content of REO dopant (both CeO_2 and Er_2O_3) the tetragonal phase is favored with respect to the monoclinic one, and the samples containing 5 mol% of RE are mainly constituted by t-ZrO_2. Carefully analyzing the diffractograms, it is possible to observe that in the case of the m-ZrO_2 the width of the diffracted peaks is not constant with the angle of diffraction, which means that an anisotropy in the crystallite dimensions occurs. Therefore, for all materials, the monoclinic phase crystallites do not show the same dimensions in the different crystalline direction, i.e. the crystallites cannot be considered as "spheres" but they probably have a different shape (e.g. flower like or elliptic).

The influence of RE doping on the optical absorption of the various samples has been investigated by Diffuse Reflectance (DR) UV-Vis spectroscopy. Figure 2 compares the spectra recorded for pure zirconia with those of the variously doped samples Ce (panel a), and Er (panel b).

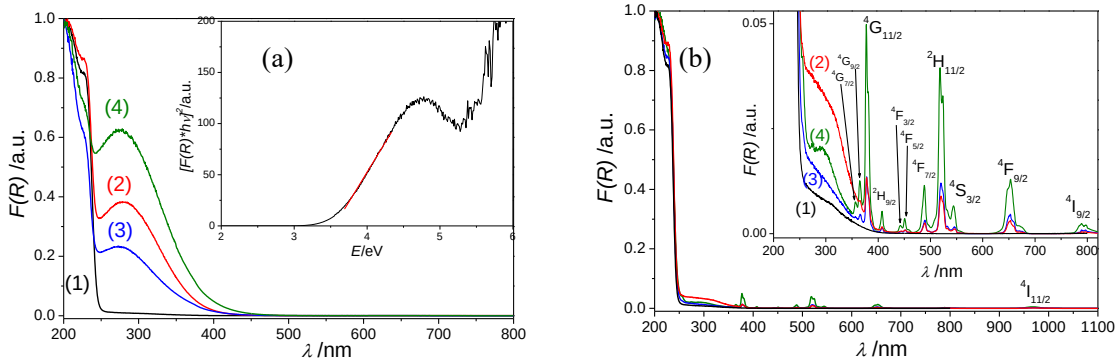

Figure 2. Diffuse reflectance absorbance spectra of 1) pure ZrO_2 (black) and RE-doped ZrO_2 (panel a: RE=Ce, panel b: RE=Er) with increasing concentration of RE dopant: 2) 0.5 mol% (red), 3) 1 mol% (blue), 4) 5 mol% (green). Inset of panel (a): Tauc plot of CZ5. Inset of panel (b): magnification of the 200-800 nm region.

The spectrum of bare ZrO_2, reported for the sake of comparison in both panels of Fig. 2, is well known and is dominated by the band gap transition occurring at about 250 nm (5 eV) that is due to the electrons excitation from the valence band (VB) to the conduction band (CB). A very weak absorption between 250 nm and 350 nm is also present, which is due to traces of point defects always present in the bare material [17]. No absorption is observed in the visible region.

The use of different types and amounts of the dopant dramatically affects the optical properties of the materials. The effect of rare earth ions addition on these properties is however very different in the two cases. In the case of Ce-doped ZrO_2, the presence of the dopant strongly influences and apparently modifies the VB → CB transition of zirconia. It is easy to observe (Fig. 2a) an effect describable as a progressive red shift of the oxide absorption edge that increases with increasing the cerium percentage. The samples indeed change their color: from pure white of the bare zirconia to a primrose yellow for the CZ5 sample. To evaluate the entity of this red shift, we calculated the energy gap (E_g) value for all samples using the Tauc plot. Eg is calculated by linearization of the plot reporting $(\alpha h\nu)^2$ vs $h\nu$ typical of direct band gap transitions [18]. The results are reported in Table 1.

Table 1. Nominal content of the RE ZrO_2 samples; calculated Energy gap (E_g) value, specific surface area S_{BET}, amount of hole center generated by visible irradiation I (arbitrary units, see text) and discoloration

apparent kinetic constant for Ce and Er-doped ZrO_2 photocatalysts *k*

Sample	RE mol%	E_g/eV	S_{BET}/m^2/g	*I* /a.u.	*k*/min^{-1}
Z	0	5.15	44	0.10	-
EZ05	0.5	5.13	51	1.31	0.0022
EZ1	1	5.13	63	0.74	0.0018
EZ5	5	5.12	96	0.18	0.0016
CZ05	0.5	4.06	39	3.32	0.0041
CZ1	1	3.84	44	2.18	0.0034
CZ5	5	3.55	66	2.05	0.0031

As it can be seen the addition of Ce progressively narrows the E_g value, with a minimum value of 3.55 eV, which corresponds to a 1.6 eV narrowing.

If we consider Er-doped ZrO_2, the situation is completely different. There are, in this case, two distinct effects: the first one is an absorption band centered at about 290 nm which is similar, tough far less intense, to that observed in the same region for Ce-ZrO_2. This has a maximum for the EZ05 sample, then decreases in intensity for the EZ1 sample and finally increases again for the EZ5 sample. The second effect is the presence of a multitude of absorption bands related to the states of Er^{3+}. The intensity of these bands increases when increasing the Er content and their presence indicates that Er ions are well diluted in the matrix and preserving their optical properties [11, 19, 20]. These bands are indexed in the inset of figure 2, panel (b), according to the nomenclature $^{2S+1}L_J$, where *S* is the spin quantum number of the ion, *L* is the total orbital angular momentum quantum number (the state symbol is *S* if *L* = 0, P if *L* = 1, D if *L* = 2, F if *L* = 3, G if *L* = 4, H if *L* = 5, I if *L* = 6 and K if *L* = 7) and *J* is the quantum number, resulting from the vector addition of *S* and *L*. The materials' energy gap in the case of Erbium doping is almost unmodified, preserving its value around 5.1 eV.

EPR is a suitable technique to monitor the charge separation processes. This was first shown, in the case of TiO_2, by the work of Graetzel and Howe [21, 22] and by that of the Thurnauer group [23] who

were able to directly monitor the spectral trace of both excited electrons and holes upon irradiation of a colloidal suspension of the oxide in water. The same experiment can be performed, though less efficiently, under vacuum as shown by some of us in the case of titania based photoactive solids [5, 24]. The direct charge separation is obtained irradiating in situ the solid at the temperature of liquid nitrogen to avoid the rapid recombination of the carriers.

In the case of a generic oxide the reaction occurring is :

$$MeO_X + h\nu \rightarrow e^-_{(CB)} + h^+_{(VB)} \qquad (1)$$

If the two photogenerated charge carriers are stabilized by the solid this occurs at different sites of the oxide, usually a cation for the electron and an oxide anion for the hole. In our case, formation of Zr^{3+} ($Zr^{4+} + e^- \rightarrow Zr^{3+}$) and O^- ($O^{2-} + h^+ \rightarrow O^-$), which are both paramagnetic and EPR visible, is expected. Nevertheless, if the photogenerated charge carriers are not stabilized but remain highly mobile, they can escape from EPR detection. Whether the carriers localize or not depends on many variables, including the synthesis procedure.

Figure 3 shows the behaviour of pristine zirconia under irradiation. Trace a is the spectrum of the material in the dark, which, in fact, already contains some defects. Indeed an isotropic signal assigned to free electrons at grain boundaries [17] is detected. Trace b reports the behaviour of the oxide under UV-Vis (complete emission spectrum of the lamp) irradiation. The UV-Vis irradiation leads to a clear evidence for the formation of photogenerated holes. On the other hand for this sample (hydrothermally prepared) there is no evidence for localized electrons (as it happens for instance in the case of sol-gel prepared zirconia [17]). This does not necessarily mean that there are no electrons, but that they escape from EPR detection. We can indirectly see the photogenerated electrons by irradiating the sample in presence of molecular oxygen: the electrons that reach the surface are able to react with it and form the paramagnetic superoxide anion, $O_2^{-\cdot}$ [25]. For sake of brevity and since the behaviour of photogenerated electrons is beyond the purpose of this paper this experiment is not reported.

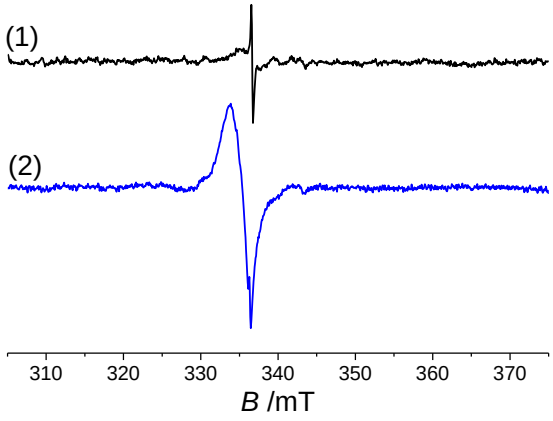

Figure 3. EPR spectra recorded at 77K of bare ZrO_2: 1) background, 2) UV-Vis irradiated.

Preliminary results from our group have shown some photoactivity under visible light of a Ce doped ZrO_2 material prepared via sol-gel [10]. Figure 4 reports the effect of the visible irradiation on the pure and 0.5% Ce doped ZrO_2 samples.

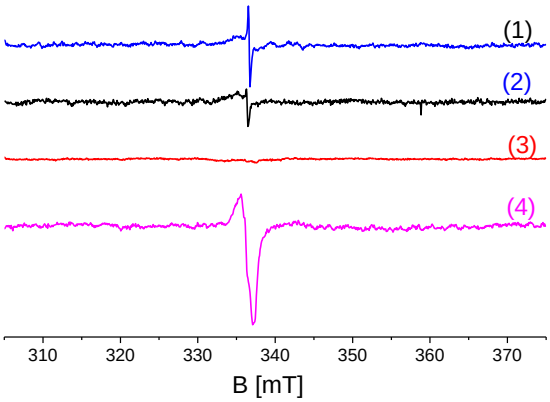

Figure 4. EPR spectra recorded at 77K of pure ZrO_2 (1, 2) and CZ05 (3, 4), before (1, 3) and after (2, 4) 15 minutes of irradiation with visible light (λ>400nm).

No effect is observed upon irradiation of ZrO_2 with visible light (λ>400 nm, i.e. $h\nu$<3.1 eV, fig. 4 line 2) whereas in the case of CZ05 the same kind of light induces the formation of a signal in the region at g> 2.0 typical for holes stabilized on oxygen ions (i.e. O^- ions) [26], fig. 4 trace 4. The observed effect is recorded for all the doped samples with lower intensity. The relative amount of holes photogenerated by visible light (and in the same experimental conditions) has been evaluated by double integration of the corresponding (first derivative) EPR signal and is reported in Table 1 (third column). It is easily deduced

from the table that Ce doped materials are systematically more active than the Er doped ones. Furthermore for both series of samples the photoactivity in hole generation decreases by increasing the REO loading. In other words, the 0.5 mol% materials are in both series the most active ones.

Preliminary experiments were carried out in order to verify that MB dye was degraded by heterogeneous photocatalytic process under visible light (λ>400 nm, see experimental). In the absence of photocatalyst, no significant decrease in MB concentration was observed during 3 h of illumination. In particular, MB discoloration was less than 7%. So, photolysis phenomena occur but at a limited extent [27].

The behavior of MB discoloration under LED-generated visible light is reported in Figure 5 for the six Ce and Er-doped ZrO_2 samples explored in this work. The Ce-doped samples (more active from the point of view of the formation of holes) clearly show a better oxidation activity towards Methylene Blue (vide infra).

The most active material (CZ05) decomposes 50% of the MB dye in three hours. The activity of Er doped samples in the same time interval is about half of that shown by Ce-ZrO_2.

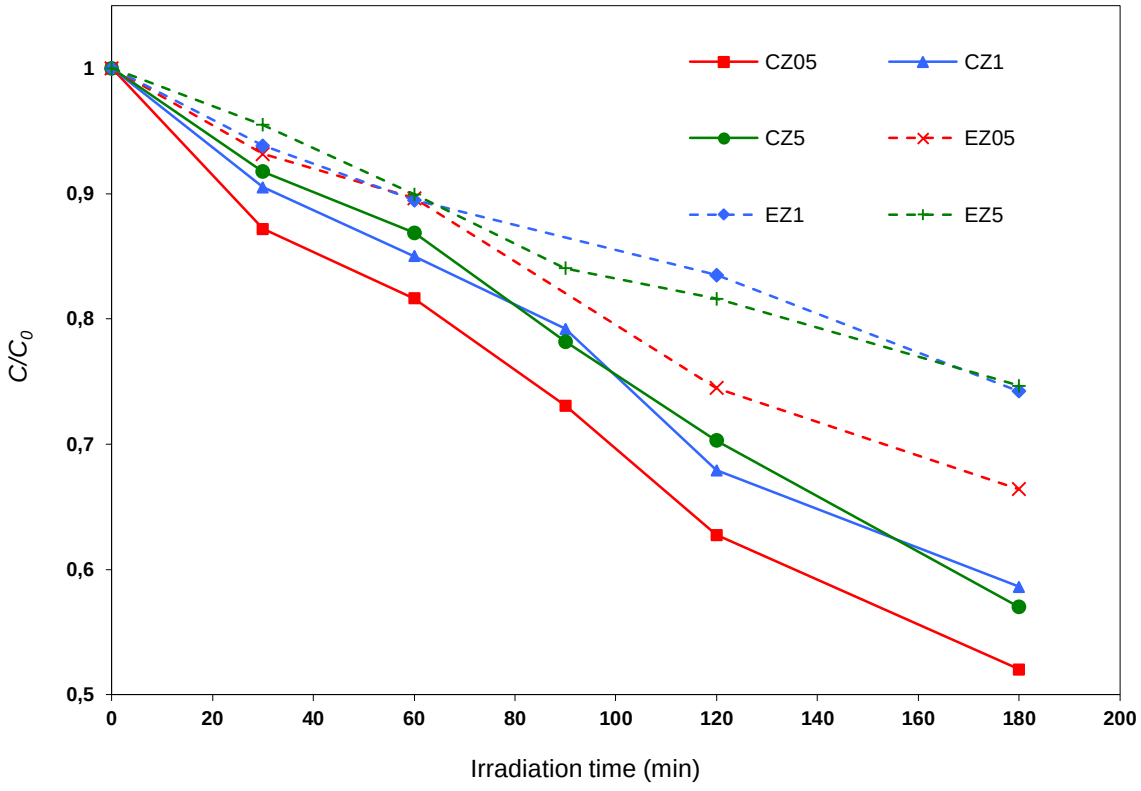

Figure 5. Behaviour of MB discoloration for Ce and Er-doped ZrO_2 photocatalysts; photocatalyst dosage:

3 g/L; MB initial concentration: 7 ppm; pH: 6.5; temperature: 303 K..

In particular, considering Ce-doped ZrO_2, the highest discoloration activity was obtained on CZ05 sample, whereas CZ1 and CZ5 showed a very similar activity. The same trends are observed for Er-doped ZrO_2 samples. In fact, EZ05 is more active than EZ1 and EZ5, which in turn evidence almost the same MB discoloration ability.

The photocatalytic discoloration process can be described by a first-order kinetic equation (Eq. 1) with respect to the concentration of MB dye [28].

During irradiation, the mass balance on MB present in the aqueous solution can be written as:

$$\frac{dC(t)}{dt} = -k \cdot C(t) \qquad (2)$$

Where:

$C(t)$: concentration of MB at given reaction time, [mg L^{-1}]

k: discoloration apparent kinetic constant, [min^{-1}]

The initial conditions are:

$t=0 \qquad C=C_0^*$

Where C_0^* is the MB concentration after the starting period in dark.

Eq. 2 was solved by the Euler iterative method to identify the discoloration apparent kinetic constant k, using a nonlinear regression analysis of the experimental data reported in Figure 5. The nonlinear regression procedure was performed using the least-squares approach, based on the minimization of the sum of squared residuals between the experimental data and the values given by the mathematical model. The obtained values of k are reported in Table 1 (last column).

CZ05 catalyst showed the highest value of k while EZ05 presented a discoloration apparent kinetic constant about two times lower than that obtained for CZ05.

Generally, the photocatalytic degradation of organic pollutants in aqueous phase is believed to be initiated by the $^{\bullet}OH$ radical, which is formed through the oxidation of H_2O by holes (h^+_{vb}) and can oxidize almost all organic compounds [28]. In the case of MB, the first step of the dye degradation is its

discoloration. because of the generation of leuco MB form (LMB) that is colourless.

Figure 6 reports the discoloration apparent kinetic constant values of the photocatalytic process in visible light as a function of the amount of photogenerated holes (Table 1) for all samples.

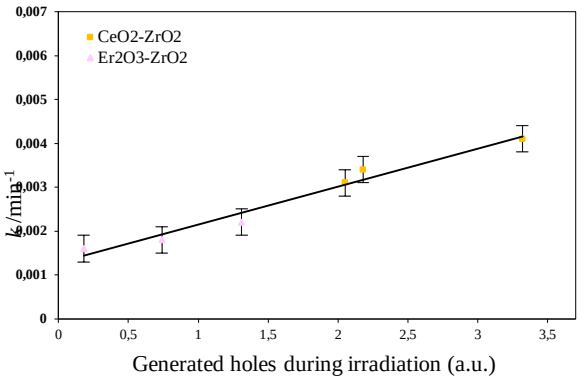

Figure 6. Behavior of *k* for Ce and Er-doped ZrO_2 photocatalysts as a function of generated holes

It is possible to observe a nice linear correlation between the two kind of values, that holds for both photocatalytic families. This result is certainly most important since it unambiguously establishes a direct correlation between the EPR evaluated holes amount and the photocatalytic activity. To the best of our knowledge this is the first correlation of this type available in the literature. Moreover this trend is common for both photocatalysts families, so discoloration apparent kinetic constant is correlated directly with the amount of photogenerated holes, as measured by EPR.

To understand the experimental results related to the MB discoloration (Figure 6), the following reaction mechanism of photocatalytic degradation of MB in presence of semiconductors particles has to be considered [29].

$^{1}MB_{0} + h\nu \rightarrow {}^{1}MB_{1}$ (Singlet excited state) (3)

$^{1}MB_{1} \rightarrow {}^{3}MB_{1}$ (Triplet excited state) (4)

Photocatalyst $+h\nu \rightarrow e^{-}_{cb} + h^{+}_{(VB)}$ (5)

$h^{+} + OH^{-}_{surf} \longrightarrow {}^{\bullet}OH$ (6)

$h^{+} + O^{2-}_{surf} \rightarrow O^{-}_{surf}$ (7)

$O^{-}_{surf} + H_2O \rightarrow OH^{-}_{surf} + {}^{\bullet}OH$ (8)

$O^{-} + {}^{3}MB_{1} \rightarrow LMB$ (9)

$LMB + {}^{\bullet}OH \rightarrow INTERMEDIATES \rightarrow CO_2 + H_2O$ (10)

Under light irradiation, $^1MB_0$ gives rise to its excited singlet state (Eq. 3), where the electron is promoted in the same spin orientation as it was in the ground state (paired). Then $^1MB_1$ is excited to a higher energy level, the triplet states of the dye $^3MB_1$ (Eq. 4), where the promoted electron has the same spin orientation (parallel) to the other unpaired electron.

In parallel, the photocatalyst utilizes the light energy to excite its electron from the valence band to the conduction band (Eq. 5); thus, leaving behind a hole. This hole localizes onto both O^{2-} and OH^- ions to generate O^- ions and •OH radicals (Eq.s 6-8). The O^- radical ion react with $^3MB_1$ to give the corresponding leuco MB form (LMB) (Eq. 9), which is colourless. Finally, the degradation pathway of the LMB gives intermediates ending up in the formation of CO_2 and H_2O [30] (Eq. 10).

As expected the discoloration process is related to the Eq. 9 and it essentially depends on the number of holes produced during the irradiation of the photocatalyst (Eq.5).

In this way, it is possible to explain the linear correlation between the discoloration rate and the amount of generated holes.

Considering the existence and the role played by the colourless leuco form of the dye (LMB) as well as the possible formation of colourless intermediates, the simple discolouration of the solution does not necessarily correspond to the oxidation and mineralization of the dye. For this reason, in order to ascertain the efficiency of the photocatalysts in the “true” mineralization of the dye, a Total Organic Carbon (TOC) analysis was also carried out on the various systems. The results of this analysis are summarized in Fig. 7 where TOC removal data are coupled with MB discoloration ones.

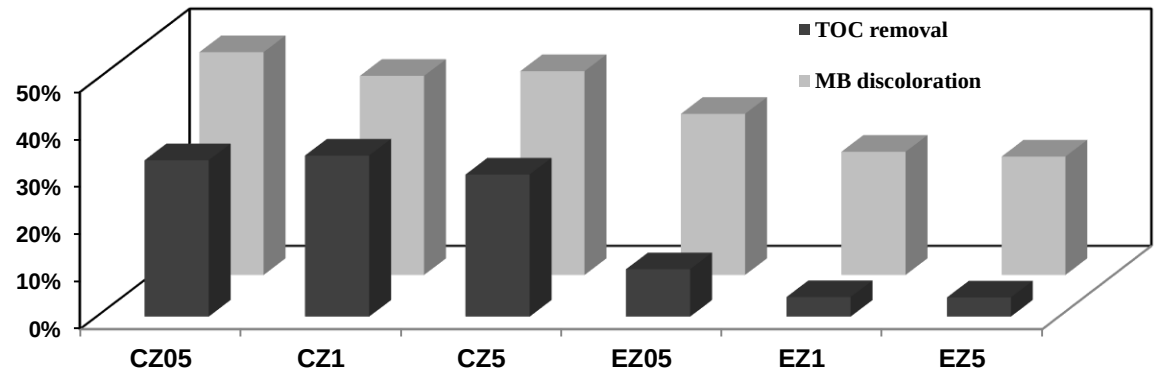

Figure 7: Photocatalytic performances in the MB photocatalytic discoloration and TOC removal after 2 hours of visible light irradiation

The data compared in Fig. 7 indicate that a fraction of the observed discoloration is due to the formation of the leuco form of the dye and/or of colourless intermediates. This fraction is particularly high in the case of the EZ series, while it is lower in the case of the CZ systems. These latter catalysts appear thus to be effective in a true mineralization of MB with the two systems at lower loading (CZ05, CZ1) showing a similar efficiency.

4. Conclusions

The introduction of new electronic states in high band gap semiconductors like ZrO_2, realized by doping with rare earth elements like Ce and Er, leads to new photocatalysts able to absorb some portions of visible light, and to perform, in this way, a classic electron-hole separation. Ce and Er- doped ZrO_2 resulted photoactive in methylene blue removal in aqueous solution promoted by white LEDs light. The optimal composition for the two different families of photocatalysts was individuated. Photocatalytic activity results, rigorously obtained under visible light irradiation, showed that the methylene blue discoloration rate is a function of the number of holes produced during the irradiation of the photocatalyst. CZ05 catalyst showed the highest value of discoloration rate while EZ05 presented a discoloration apparent kinetic constant about two times lower than that one obtained for CZ05. Ce-doped ZrO_2 showed also the highest mineralization activity.

This uncommon behavior for an insulator oxide like ZrO_2 (with a band gap of more than 5 eV) has been already explained elsewhere [10]. Intra band gap states formed by the lanthanides f orbitals are the responsible for the "double jump" absorption leading to excitation of the electrons in the CB. The materials

here described can be assumed to well describe the third generation catalysts theorized by Emeline and Serpone [7, 8].

With the results reported in the present paper the systems based on RE doped ZrO_2 (and in particular Ce-ZrO_2) end to be a simple proof of concept and enter in the domain of photocatalytic systems active in visible light. Further work is needed both to fine tune the composition (and the preparation method) of the photoactive materials and to extend its application by using true solar light in photocatalytic reactions.

Acknowledgments

Technical assistance, material support, and other help or advice may be acknowledged briefly in this section (excluding financial support, which should appear in the footnote on the title page).

References:

[1] G. Palmisano, A. Albini, G. Marcì, L. Palmisano, D. Ravelli. New synthetic routes in heterogeneous photocatalysis. In RSC Energy and Environment Series, Royal Society of Chemistry, 2016. 303-344

[2] H. Zhang, G. Chen, D.W. Bahnemann. J. Mater. Chem. 19 (2009) 5089-5121

[3] D. Spasiano, R. Marotta, S. Malato, P. Fernandez-Ibañez, I. Di Somma. Appl. Catal., B 170 (2015) 90-123

[4] S. Livraghi, M.C. Paganini, E. Giamello, A. Selloni, C. Di Valentin, G. Pacchioni. J. Am. Chem. Soc. 128 (2006) 15666-15671

[5] G. Barolo, S. Livraghi, M. Chiesa, M.C. Paganini, E. Giamello. J. Phys. Chem. C 116 (2012) 20887-20894

[6] R. Asahi, T. Morikawa, T. Ohwaki, K. Aoki, Y. Taga. Science 293 (2001) 269-271

[7] A.V. Emeline, V.N. Kuznetsov, V.K. Ryabchuk, N. Serpone. Environ. Sci. Pollut. Res. 19 (2012) 3666-3675

[8] N. Serpone, A.V. Emeline. J. Phys. Chem. Lett. 3 (2012) 673-677

[9] C. Gionco, A. Battiato, E. Vittone, M.C. Paganini, E. Giamello. J. Solid State Chem. 201 (2013) 222-228

[10] C. Gionco, M.C. Paganini, E. Giamello, R. Burgess, C. Di Valentin, G. Pacchioni. J. Phys. Chem. Lett. (2014) 447-451

[11] J. Reszczynska, T. Grzyb, J.W. Sobczak, W. Lisowski, M. Gazda, B. Ohtani, A. Zaleska. Appl. Catal., B 163 (2015) 40-49

[12] M. Gratzel. Nature 414 (2001) 338-344

[13] V. Vaiano, O. Sacco, D. Sannino, P. Ciambelli. Chem. Eng. J. 261 (2015) 3-8

[14] V. Vaiano, O. Sacco, M. Stoller, A. Chianese, P. Ciambelli, D. Sannino. Int. J. Chem. React. Eng. 12 (2014)

[15] V. Vaiano, O. Sacco, D. Sannino, P. Ciambelli. Appl. Catal., B 170 (2015) 153-161

[16] D. Sannino, V. Vaiano, P. Ciambelli, L.A. Isupova. Chem. Eng. J. 224 (2013) 53-58

[17] C. Gionco, M.C. Paganini, E. Giamello, R. Burgess, C. Di Valentin, G. Pacchioni. Chem. Mater. 25 (2013) 2243-2253

[18] G. Martra, E. Gianotti, S. Coluccia, in: Metal Oxide Catalysis, Wiley-VCH Verlag GmbH & Co. KGaA, 2009. pp 51-94

[19] W.T. Carnall. Handbook on the Physics and Chemistry of Rare Earths 3 (1979) 171-208

[20] W.T. Carnall, P.R. Fields, R. Sarup. J. Chem. Phys. 57 (1972) 68-75

[21] R.F. Howe, M. Gratzel. J. Phys. Chem. 89 (1985) 4495-4499

[22] R.F. Howe, M. Gratzel. J. Phys. Chem. 91 (1987) 3906-3909

[23] O.I. Micic, Y.N. Zhang, K.R. Cromack, A.D. Trifunac, M.C. Thurnauer. J. Phys. Chem. 97 (1993) 13284-13288
[24] M. Chiesa, M.C. Paganini, S. Livraghi, E. Giamello. Phys. Chem. Chem. Phys. 15 (2013) 9435-9447
[25] N. Siedl, M.J. Elser, J. Bernardi, O. Diwald. J. Phys. Chem. C 113 (2009) 15792-15795
[26] M. Chiesa, E. Giamello, C. Di Valentin, G. Pacchioni. Chem. Phys. Lett. 403 (2005) 124-128
[27] O. Sacco, M. Stoller, V. Vaiano, P. Ciambelli, A. Chianese, D. Sannino. Int. J. Photoenergy (2012)
[28] J.L. Wang, L.J. Xu. Crit. Rev. Env. Sci. Technol. 42 (2012) 251-325
[29] D.K. Sharma, H.S. Sharma. Know res. 2 (2015) 10-14
[30] A. Houas, H. Lachheb, M. Ksibi, E. Elaloui, C. Guillard, J.-M. Herrmann. Appl. Catal., B 31 (2001) 145-157